Full-field optical coherence tomography with a complimentary metal-oxide semiconductor digital signal processor camera

Patrick Egan
University of Limerick
Optical Communications Research Group
Limerick, Ireland
and
European Commission Joint Research Centre
Institute for Health and Consumer Protection
Photonics Sector
Ispra, Italy
E-mail: Patrick.Egan@ul.ie

Fereydoun Lakestani
Maurice P. Whelan, MEMBER SPIE
European Commission Joint Research Centre
Institute for Health and Consumer Protection
Photonics Sector
Ispra, Italy

Michael J. Connelly, MEMBER SPIE
University of Limerick
Optical Communications Research Group
Limerick, Ireland

Abstract. Full-field optical coherence tomography (OCT) using a complementary metal-oxide semiconductor (CMOS) camera with an integrated a digital signal processor (DSP) is demonstrated. The CMOS-DSP camera employed is typically used in machine vision applications and is based on an array of 1024×1024 direct readout pixels that are randomly addressable in space and time. These characteristics enable the camera to be used as a fast full-field detector in carrier-based optical metrology systems. The integrated DSP facilitates basic signal processing including real-time filtering and undersampling. The optical setup used to implement this OCT method is composed of a free-space Michelson interferometer and a superluminescent diode (SLD) light source, with an electromechanical shaker for depth scanning. Unlike classical OCT approaches, however, the setup does not require any electromechanical device for lateral scanning. A 64×30 pixel region of interest was imaged at 235 frames/s and sampled in depth, corresponding to a volumetric measurement of $875 \times 410 \times 150$ μm. Measurements carried out on a simple calibration specimen indicated lateral and axial resolutions of 14 and 22 μm, respectively. The presented approach offers an inexpensive and versatile alternative to traditional OCT systems and provides the basis for a functional machine vision system suitable for industrial applications.
 [DOI: 10.1117/1.2158968]

Subject terms: optical coherence tomography; full field; electronic scanning; complementary metal-oxide semiconductor camera; carrier-based detection.

Paper 050054R received Jan. 21, 2005; revised manuscript received Jun. 10, 2005; accepted for publication Jun. 10, 2005; published online Jan. 24, 2006.

1 Introduction

Since its foundation[1,2] the paramount preoccupation with optical coherence tomography (OCT) has been higher resolution in 2-D cross-sectional imaging for biomedical applications. This has stimulated OCT designs with complex optical setups,[3,4] expensive light sources,[5–7] and complicated lateral scanning of the sample under test.[8–10] A simplistic solution for industrial 3-D imaging, using lower specification full-field OCT, has been largely ignored.

Systems based on single-point, or flying-spot time domain OCT must scan the sample in two lateral dimensions and reconstruct a 3-D image using depth information obtained by coherence gating through an axially scanning reference arm. Two-dimensional lateral scanning has been electromechanically implemented by moving the sample[11] using a translation stage, and using a novel microelectromechanical system scanner.[12] These approaches are slow, complex, and costly due to the drawbacks of a 2-D electromechanical scanner.

Parallel OCT using a charge-coupled device (CCD) camera has been used in which the sample is full-field illuminated and *en face* imaged with the CCD, hence eliminating the electromechanical lateral scan. By stepping the reference mirror and recording successive *en face* images a 3-D representation can be reconstructed. Three-dimensional OCT using a CCD camera was demonstrated in a phase-stepped technique,[13] using geometric phase shifting with a Linnik interferometer,[14] utilizing a pair of CCDs and heterodyne detection,[15] and in a Linnik interferometer with an oscillating reference mirror and axial translation stage.[16] Central to the CCD approach is the necessity for either very fast CCDs or carrier generation separate from the stepping reference mirror to track the high-frequency OCT carrier, hence adding cost and complexity to the system. Furthermore, an abundance of often redundant information exists when a 3-D tomograph is reconstructed from many fixed region of interest (ROI) CCD frames, requiring external storage and processing hardware.

A 2-D smart detector array, fabricated using a 2 μm CMOS process, was used to demonstrate[17] full-field OCT. Featuring an uncomplicated optical setup, each pixel of the 58×58 pixel smart detector array acted as an individual photodiode and included its own hardware demodulation circuitry. The weaknesses of this CMOS method are the cost of the design and fabrication of a custom-built detector array, and the inflexibility of hardware-based demodulation. Moreover, the hardware demodulation circuitry surrounding the photodiode of this CMOS pixel reduces its fill factor, i.e., the ratio of photodiode surface area to pixel area.

Full-field laser interferometry utilizing a programmable CMOS-DSP (digital signal processor) camera has been reported.[18] The system performed 2-D lateral scanning by electronically addressing successive pixels, exploiting the random pixel accessibility inherent to the camera sensor. A further benefit of the random pixel accessibility was ROI-only imaging which enables faster frame rates. Demodulation was performed digitally using the DSP of the camera. This work established the CMOS-DSP camera as a flexible and inexpensive solution for automated high-precision optical metrology.

This paper reports full-field OCT of a rough aluminum sample using a programmable CMOS-DSP camera. In a very simple optical setup, 2-D lateral scanning was performed electronically by addressing the pixels of the camera. Carrier-based detection and processing of the OCT signal were carried out digitally. The approach exhibits ROI full-field imaging, enabling extremely fast frame rates by avoiding redundant information acquisition and processing. The paper demonstrates a progressive 3-D OCT imaging system of novel simplicity, functionality, and versatility, where, contrary to often inflexible higher resolution biomedical OCT, the aim is to exploit a reasonably priced noninvasive 3-D imaging technique for industrial measurement applications.

2 Low-Coherence Interferometry with a CMOS Camera

The basis of OCT is low-coherence interferometry[19–21] and compiling a tomograph of a sample microstructure by reconstructing its reflection map. In a Michelson interferometer with a partially coherent light source, interference is achieved only when the reference and sample path lengths are matched within the coherence length of the light source. If the path length of one arm is varied, a low-coherence interference envelope of maximum amplitude corresponding to the point of path length matching, is produced. The envelope amplitude, superimposed on a carrier relates to reflection coefficient of the sample surface. A cross-sectional tomograph, or B-scan, is achieved by laterally scanning a sample and combining each point-spatial reflection map. A 3-D representation requires lateral scanning in two dimensions.

Essential to the implementation of two-dimensional electronic pixel scanning is random pixel access of the imaging sensor. The CMOS-DSP camera (iMVS-155, AKAtech SA, Switzerland) used in this experiment features a 1024×1024 logarithmic CMOS sensor,[22,23] an analog-to-digital converter (ADC), a DSP, a super video graphics array (SVGA) output, eight digital input/output lines, an RS-232 communication port, and static random access memory (SRAM), all in a compact stand-alone device. Individual and groups of pixels can be randomly addressed in space and time and real-time processed by rapidly uploading a C program from an external computer to the internal DSP. The output from the camera is then displayed on a VGA monitor or uploaded to the external computer.

A characteristic of the CMOS pixel is its logarithmic voltage response to light intensity, as shown in Fig. 1, which is approximated within ±3% in the range 10^{-4} to 10^{2} W m^{-2}, as

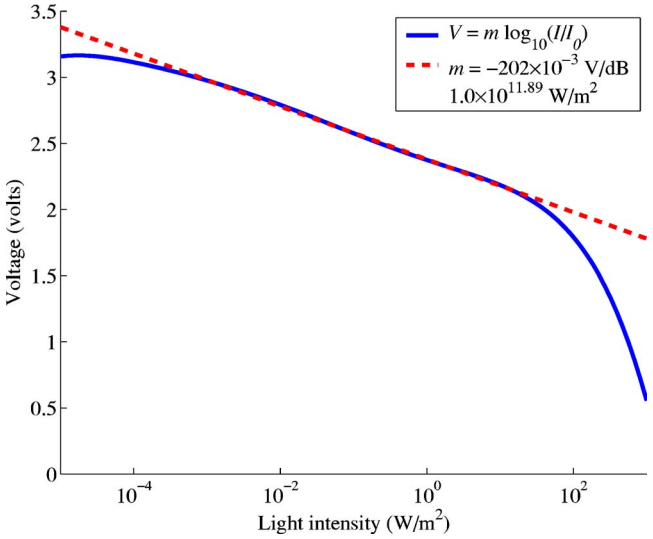

Fig. 1 Logarithmic pixel response of the CMOS-DSP camera. The output voltage is converted to an 8-bit value by the camera's internal ADC.

$$V = m \log_{10}\left(\frac{I}{I_0}\right), \tag{1}$$

where I is the light intensity on the pixel, and m and I_0 are constants. Although the logarithmic response makes the camera sensitive to light intensity over an impressive 120 dB range, Eq. (1) has significant implications when the camera is used as a full-field detector in a carrier-based interferometric imaging system. The interference of two partially coherent light beams can be expressed in terms of the source intensity I_S as

$$I = k_1 I_S + k_2 I_S + 2[(k_1 I_S)(k_2 I_S)]^{1/2} \operatorname{Re}[\gamma(\tau)], \tag{2}$$

where $k_1 + k_2 \approx 1$ represents the interferometer beamsplitting ratio; and $\gamma(\tau)$ is called the complex degree of coherence, i.e., the interference envelope and carrier dependent on the reference arm scan or time delay τ, and whose recovery is of interest in OCT. Substituting Eq. (2) for I in Eq. (1) results in

$$V = m \log_{10}\left\{\frac{I_S}{I_0}(k_1 + k_2) + \frac{I_S}{I_0} 2(k_1 k_2)^{1/2} \operatorname{Re}[\gamma(\tau)]\right\}. \tag{3}$$

Factorizing, and using the logarithm property, the output pixel voltage becomes

$$V = m \log_{10}\left(\frac{I_S}{I_0}\right) + m \log_{10}\{(k_1 + k_2) + 2(k_1 k_2)^{1/2} \operatorname{Re}[\gamma(\tau)]\}. \tag{4}$$

From Eq. (4) it is clear that the magnitude of the time-dependent component of the signal $\gamma(\tau)$ included in the second term is independent of source intensity I_S due to the logarithmic response property of the CMOS sensor. Hence, as a consequence of the CMOS-DSP camera's logarithmic response, increasing the source intensity acts simply as a dc offset and does not increase the coherence envelope mag-

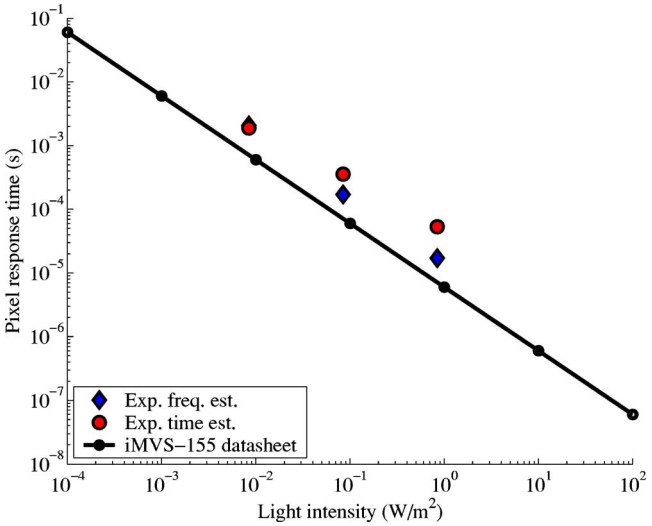

Fig. 2 Pixel response time and light intensity. At low light intensities, the pixel response time is longer, corresponding to a lower cutoff frequency.

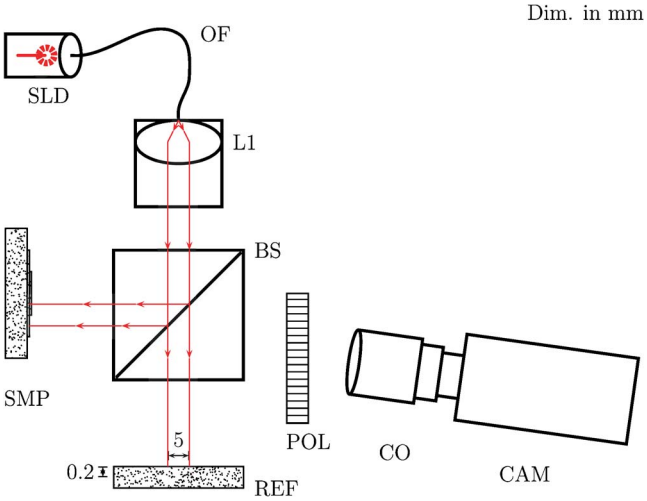

Fig. 3 Full-field OCT optical setup. Components include superluminescent diode (SLD), convex lens (L1), 50/50 beamsplitter (BS), polarizer (POL), camera objective (CO), and CMOS-DSP camera (CAM). The reference (REF) and sample (SMP) are of the same rough aluminum finish.

nitude. Furthermore, achieving a higher ac signal requires a higher ratio of ac component with respect to the dc component, i.e., higher visibility, since in this camera, the equivalent noise voltage at the pixel output is almost independent of light intensity and a higher signal at pixel output means a higher signal-to-noise ratio (SNR).

The logarithmic response is a consequence of the flow of the photocurrent through a logarithmic resistive load. Associated with this logarithmic load and the circuit capacitance is a pixel response time dependent on light intensity. The response time was analyzed in the time and frequency domains, using stepped intensity and swept sinusoidal frequency modulation of a 720 nm laser diode light source, respectively. The time-domain response exhibited exponential rise and decay, and the frequency analysis revealed a lowpass filter characteristic, with a −3 dB cutoff frequency. The relationship between pixel response time and light intensity is shown in Fig. 2. Because the slope is 1 and the scale of both axes is logarithmic, the time response is linearly proportional to light intensity. As light intensity is decreased, the pixel response time increases. With the low-light intensities of an OCT signal, the response time must be considered. If the frequency of the optical carrier, determined by the velocity of the scanning arm, is greater than the cutoff frequency of the pixel at a particular intensity, the signal will be attenuated and the SNR is reduced. Hence, in low-coherence interferometry, the characteristics of the CMOS-DSP camera impose an implicit trade-off between light intensity, scan speed, and SNR.

3 Method

3.1 *Optical Setup*

The experimental setup is shown in Fig. 3. The superluminescent diode (SLD) light source had a full width at half maximum spectral bandwidth of 25 nm centered at 830 nm and supplied 3.6 mW of power. The convex lens (L1) collimated the light to a beam diameter of 5 mm. The camera objective (CO) enabled optical zoom and focusing of the sample image onto the CMOS sensor. The three notable aspects of the setup are the off-centered camera polarizer, and rough reference surface. These measures were taken to maximize the SNR of the CMOS sensor, that is, to achieve a higher visibility or higher ac/dc ratio of the light intensity components, as discussed in the previous section. The camera was off-centered to prevent parasitic dc light reflections from the beamsplitter. For each pixel there is a given orientation of the polarizer that maximizes the visibility and hence, the presence of the fixed polarizer improves the SNR for some pixels. The rough reference surface, i.e., the same as the sample surface, facilitated a maximum visibility.

The sample was axially translated using an electromechanical minishaker (type 4810, Brüel & Kjaer, Denmark) with a triangle waveform at a speed of 120 μm/s. A customized program was uploaded to the camera accessing and processing a region of 64×30 pixels, corresponding to 875×410 μm on the sample. All data were stored on the internal memory of the camera. A LabVIEW interface ran on an external computer to generate the triangle waveform to drive the minishaker and digitally trigger the camera acquisition using one of the camera's IO ports. When complete, the data were downloaded from the camera memory to the external computer for 3-D presentation.

3.2 *Sample Specification*

The sample (shown in Fig. 4) was a rough aluminum surface of two concentric circle steps, machined to a depth of $\approx$100 μm with a rough surface ($\gg\lambda_{SLD}$) finish. The camera was focused to the lower left quadrant of the 5 mm radius step and a ROI of 64×30 pixels was chosen on the CMOS sensor to overlap the step transition. The sample was thought to mimic the very low reflectivity of a typical nonspecular surface such as a semiconductor or a rough metallic surface common in industrial environments.

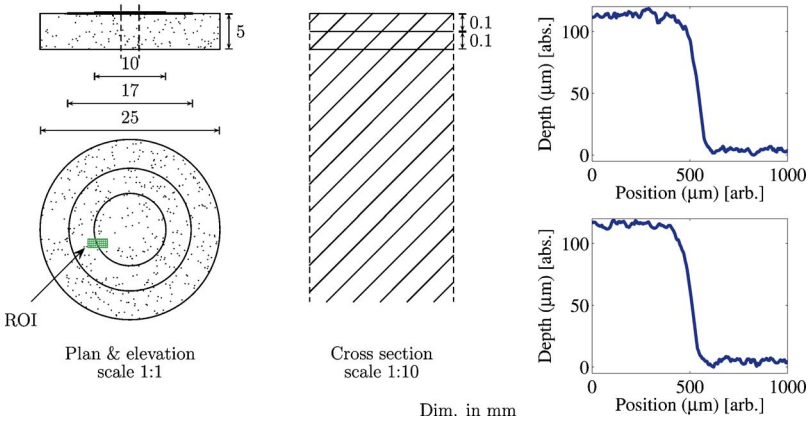

Fig. 4 Rough aluminum sample specifications. The camera ROI of 64×30 pixels (875×410 μm on the sample) is highlighted. Left: plan, elevation, and exploded cross section of sample. Right: sample profile, measured with a profilometer.

4 Results and Discussion

To highlight the signal processing capabilities of the CMOS-DSP camera, a cross-sectional tomograph of the sample, i.e., a ROI of 64×1 pixels was acquired, processed, and displayed in real time. The camera demonstrated an imaging speed of 1900 frames/s for the 64×1 pixel ROI. Three example images stepping 400 μm in the y direction are shown in Fig. 5. The images show the low-coherence interference envelope obtained at the top and bottom of the step sample as the sample is scanned in depth. Taking four samples per period of the OCT signal carrier, i.e., carrier-based detection with 4096 samples in depth, the processing consisted of bandpass filtering by a 78-tap finite impulse response (FIR) filter and taking the absolute value of the signal. The modulus of the analytic signal is the envelope. In this simple algorithm of envelope demodulation to demonstrate the on-board processing capabilities of the camera, by bandpass filtering and taking the absolute value of the experimental signal gave a frequency modulated positive envelope. Hence, the resulting dark spots in the interference envelope.

For the 3-D reconstruction, a 2-D ROI of 64×30 pixels was sampled 256 times during an axial scan, corresponding to undersampling the carrier at approximately 0.125 times the Nyquist frequency. The camera demonstrated an imaging speed of 235 frames/s for the 64×30 pixel ROI. Figure 6 shows the postprocessed reconstruction. In this postprocessing envelope demodulation algorithm, the analytic signal was bandpass filtered using frequency windowing and the corresponding analytic signal was calculated. The obtained envelope was lowpass filtered to further increase the SNR. Since the maximum value of the envelope corresponds to the point of path length matching, and hence surface location, peak detection of the envelope was used in to give the surface visualization of Fig. 6. The lateral resolution, determined by the pixel and cam-

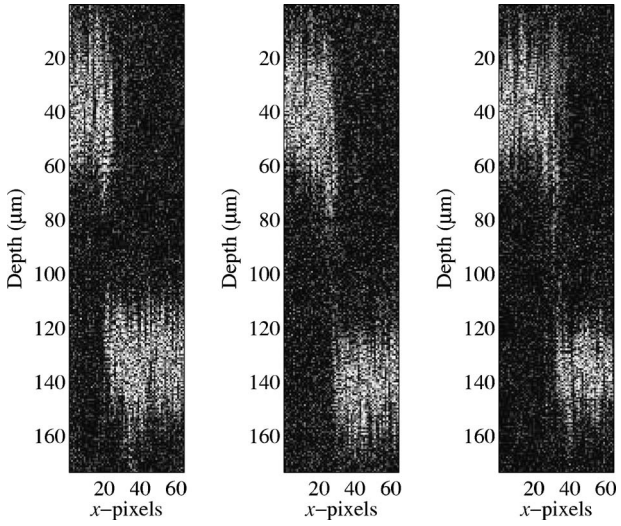

Fig. 5 Two-dimensional low-coherence reflection maps of the rough aluminum surface after real-time bandpass filtering. Lateral scan corresponds to 64 x direction pixels.

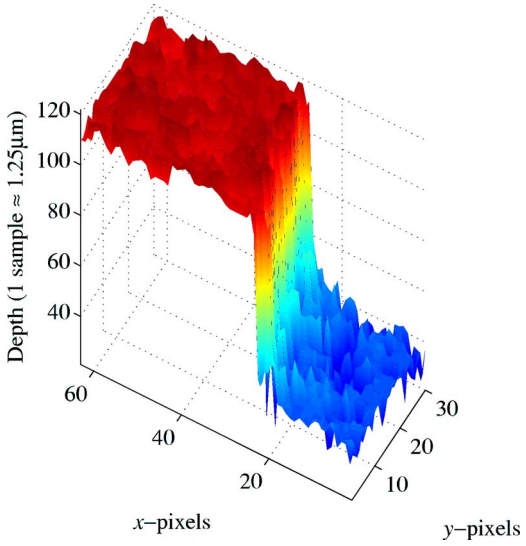

Fig. 6 Full-field OCT. Reconstructed from CMOS-DSP raw pixel data and postprocessed using MATLAB. Surface topology achieved by peak detection of the low coherence interference envelope.

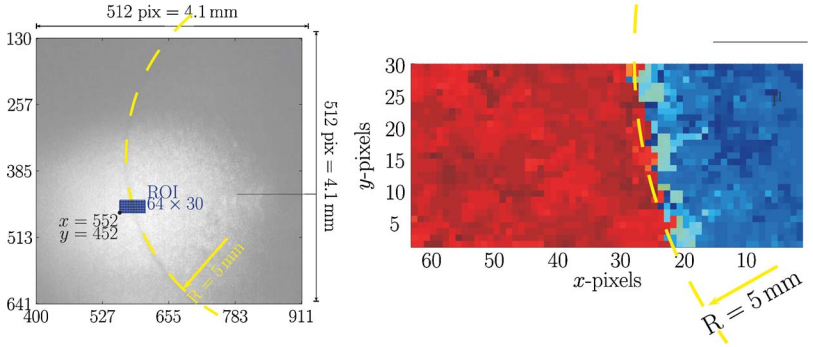

Fig. 7 *En face* comparison of actual sample image and 3-D experimental reconstruction. Left: a 512×512 pixel camera image. Right: 3-D reconstruction.

era zoom, was 14 μm, and the axial resolution, related to the coherence length of the source, was 22 μm.

A comparison of the *en face* 3-D tomograph with a 512×512 pixel *en face* camera image is shown in Fig. 7. As demonstrated, it was possible to correlate the curvature of the machined step and its 5 mm radius. Note that the *en face* camera image represents only half of the CMOS sensor area and that any shape of any size at any location on the 1024×1024 pixel array could be sampled and processed, due to the unique CMOS sensor property termed "direct readout."

The results demonstrate full-field ROI OCT of a rough metallic surface. Further to 3-D reconstruction and postprocessing, real-time 2-D processing and imaging of the surface was accomplished, using the direct readout CMOS-DSP sensor as a stand-alone imaging device. Although novel electronic pixel scanning eliminated the electromechanical lateral scanning, the logarithmic pixel response of the camera imposes a significant drawback, i.e., increasing the source power not change the SNR. However, with higher intensity, the pixel response time decreases and a faster acquisition rate can be achieved. Regardless, the results display a simplistic, versatile, and cost-effective method of noninvasive 3-D imaging for industrial applications, where a fast measurement of a small region of interest is critical, and ultrahigh resolution is irrelevant. Innovation is still required to offer random access in depth, currently restricted by the analog scanning reference arm.

5 Conclusions and Future Work

Full-field OCT without electromechanical lateral scanning using a CMOS-DSP camera and a relatively simple optical setup was demonstrated. The approach presented here offers an inexpensive and versatile alternative to traditional OCT systems and provides the basis for a functional machine vision system suitable for industrial applications. The paper demonstrated a novel simplistic, cost-effective, and versatile approach to 3D OCT using a stand-alone imaging device.

Acknowledgments

This project is supported by the University of Limerick Foundation and Enterprise Ireland International Collaboration grant. The work was undertaken within the framework of a Collaboration Agreement (No. 18697-2001-11 SOSC ISP IE) between the University of Limerick, Ireland, and the Institute for Health and Consumer Protection, EC DG-JRC, Italy. The authors would like to thank Mr. Alessio Munari of the Institute for Health and Consumer Protection, European Commission Joint Research Centre, for assistance in the profilometer measurements.

References

1. D. Huang, E. A. Swanson, C. P. Lin, J. S. Schuman, W. G. Stinson, W. Chang, M. R. Hee, T. Flotte, K. Gregory, C. A. Puliafito, and J. G. Fujimoto, "Optical coherence tomography," *Science* **254**, 1178–1181 (Nov. 1991).
2. J. A. Izatt, M. R. Hee, D. Huang, J. G. Fujimoto, E. A. Swanson, C. P. Lin, J. S. Schuman, and C. A. Puliafito, "Optical coherence tomography for medical diagnostics," in *Medical Optical Tomography: Functional Imaging and Monitoring*, G. J. Mueller et al. Eds. pp. 450–472, Bellingham, Washington (1993).
3. E. Swanson, J. Izatt, M. Hee, D. Huang, C. Lin, C. Puliafito, and J. Fujimoto, "Optical coherence tomography," in *Proc. IEEE Lasers and Electro-Optics*, pp. 656 –657, Boston, MA (1992).
4. A. M. Rollins and J. A. Izatt, "Optimal interferometer designs for optical coherence tomography," *Opt. Lett.* **24**(21), 1484–1486 (1999).
5. V. Kamensky, V. Gelikonov, G. Gelikonov, K. Pravdenko, N. Bityurin, A. Sergeev, F. Feldchtein, M. Churbanov, A. Pushkin, and I. Skripachev, "YAG:er laser system for eye microsurgery with oct monitoring," in *Proc. IEEE Lasers and Electro-Optics*, pp. 60–61, Anaheim, CA (1996).
6. E. A. Swanson, S. R. Chinn, C. W. Hodgson, A. M. Vengsarkar, S. Grubb, B. Bouma, G. Tearney, and J. G. Fujimoto, "Spectrally shaped rare-earth-doped fiber ASE sources for use in optical coherence tomography," in *Proc. IEEE Lasers and Electro-Optics*, p. 211, Anaheim, CA (1996).
7. A. Unterhuber, B. Povazay, K. Bizheva, B. Hermann, H. Sattmann, A. Stingl, T. Le, M. Seefeld, R. Menzel, M. Preusser, H. Budka, C. Schubert, H. Reitsamer, P. K. Ahnelt, J. E. Morgan, A. Cowey, and W. Drexler, "Advances in broad bandwidth light sources for ultrahigh resolution optical coherence tomography," *Phys. Med. Biol.* **49**, 1235–1246 (2004).
8. J. M. Schmitt, "OCT elastography: imaging microscopic deformation and strain of tissue," *Opt. Express* **3**(6), 199–211 (1998).
9. M. E. Brezinski and J. G. Fujimoto, "Optical coherence tomography: high-resolution imaging in nontransparent tissue," *IEEE J. Sel. Top. Quantum Electron.* **5**(4), 1185–1192 (1999).
10. S. A. Boppart, B. E. Bouma, C. Pitris, G. J. Tearney, J. G. Fujimoto, and M. E. Brezinski, "Forward-imaging instruments for optical coherence tomography," *Opt. Lett.* **22**(21), pp. 1618–1620 (1997).
11. J. M. Herrmann, M. E. Brezinski, B. E. Bouma, S. A. Boppart, C. Pitris, J. F. Southern, and J. G. Fujimoto, "Two- and three-dimensional high-resolution imaging of the human oviduct with optical coherence tomography," *Fertil. Steril.* **70**(1), 155–158 (1998).
12. J. T. W. Yeow, V. X. D. Yang, A. Chahwan, M. L. Gordon, B. Qi, I. A. Vitkin, B. C. Wilson, and A. A. Goldenberg, "Micromachined 2-D scanner for 3-D optical coherence tomography," *Sens. Actuators, A* **117**, 331–340 (2004).
13. C. Dunsby, Y. Gu, and P. M. W. French, "Single-shot phase-stepped wide-field coherence gated imaging," *Opt. Express* **11**, 105–115 (Jan. 2003).
14. M. Roy, P. Svahn, L. Cherel, and C. J. R. Sheppard, "Geometric phase-shifting for low-coherence interference microscopy," *Opt. La-*

sers Eng. **37**, 631–641 (2002).
15. M. Akiba, K. P. Chan, and N. Tanno, "Full-field optical coherence tomography by two-dimensional heterodyne detection with a pair of CCD cameras," *Opt. Lett.* **28**(10), 816–818 (2003).
16. A. Dubois, G. Moneron, K. Grieve, and A. C. Boccara, "Three-dimensional cellular-level imaging using full-field optical coherence tomography," *Phys. Med. Biol.* **49**, 1227–1234 (Mar. 2004).
17. S. Bourquin, P. Seitz, and R. P. Salathé, "Optical coherence tomography based on a two-dimensional smart detector array," *Opt. Lett.* **26**(8), 512–514 (2001).
18. M. V. Aguanno, F. Lakestani, M. P. Whelan, and M. J. Connelly, "Single pixel carrier based approach for full-field laser interferometry using a CMOS-DSP camera," *Proc. SPIE* **5251**, 304–312 (2003).
19. P. Hariharan, *Optical Interferometry*, Academic Press, Sydney (2003).
20. M. Born and E. Wolf, *Principles of Optics: Electromagnetic Theory of Propagation, Interference and Diffraction of Light*, Cambridge University Press, Cambridge (1999).
21. A. F. Fercher, W. Drexler, C. K. Hitzenberger, and T. Lasser, "Optical coherence tomography—principles and applications," *Rep. Prog. Phys.* **66**, 239–303 (Jan. 2003).
22. B. Dierickx, D. Scheffer, G. Meynants, W. Ogiers, and J. Vlummens, "Random addressable active pixel sensors," *Proc. SPIE* **5250**, 2–7 (1996).
23. S. Kavadias, B. Dierickx, D. Scheffer, A. Alaerts, D. Uwaerts, and J. Bogaerts, "A logarithmic response CMOS image sensor with on-chip calibration," *Solid State Circ.* **35**, 1146–1152 (Aug. 2000).

Patrick Egan received his BEng degree in electronic and computer engineering at the University of Limerick, Ireland in 2003. He is currently involved in doctoral research studies in a collaboration between the University of Limerick and the European Commission Joint Research Centre, Italy. His research interests include optoelectronics and signal processing.

Fereydoun Lakestani received his engineering degree from Ecole Nationale Supérieure d'Electronique et de Radioélectricité de Grenoble, France, in 1971. He taught physics and nondestructive techniques at the Institut National des Sciences Appliquées de Lyon, France, for 13 years, where he received his doctorate degree in science. He has been working at European Commission Joint Research Centre since 1984. His research activities until 1997 were in various fields of ultrasonic applications: transducers, NDT, material characterization and medicine. From 1997 to 2001 he worked on thermal waves, and since 2001 he has been involved in various applications of laser interferometry. Throughout his research activities he has acquired skill in ultrasonic, optical and thermal wave propagation and the use of electronic instrumentation, signal processing, and data analysis.

Maurice P. Whelan is currently head of the Photonics Sector of the European Commission Joint Research Centre, based in Italy and adjunct professor at the Stokes Research Institute in Ireland. He obtained his doctorate in 1994 from the University of Limerick, Ireland, in the field of computational and experimental stress analysis. Since then he has worked on the development and application of full-field optical metrology techniques, optical fiber sensing, and biomedical imaging. He is the author of 13 international patents in these fields. His current interests include interference microscopy for cell and tissue diagnostics *in vitro*, hyperspectral fluorescence imaging for endoscopy, and optical waveguide biosensors.

Michael J. Connelly received his PhD in electronic engineering from University College Dublin in 1991. Currently he is a senior lecturer in electronic engineering at the University of Limerick, where he leads a research group working on optoelectronic device modeling, all-optical signal processing using semiconductor optical amplifiers, optical coherence tomography, and optical metrology.